Nonlinear Dynamics and Chaos
Physics 134

Michelle Pichardo Munoz
University of California at Santa Cruz
Santa Cruz, CA 95064 USA

May , 2022

Abstract

The world, for a time, was assumed to be deterministic. In that, with enough calculation, we could predict the future. We know now that this is not true. That nature, human behavior, the stock market, and many other complex systems cannot dwindle to an equation where one input will give one well-behaved output. It's common knowledge that nonlinear systems can exhibit wildly different outcomes which depend highly on their initial conditions. This paper aims to examine such a system's regions of linearity, non-linearity, and chaos. We do so by comparing a 3-component linear RLC circuit with its 3-component nonlinear RLD counterpart. We exchange the linear capacitor of our RLC circuit with a diode which is governed by the nonlinear Ebers-Moll equation. Our paper describes the PDEs which govern these systems, their known solutions, and their characteristics. Likewise, we show a more qualitative analysis with a series of images identifying each region and its associated waveform. We conclude with a speculation of a strange discovery where our output signal was steady and semi sinusoidal following the near-total attenuation of our signal at the end of its chaos region.

Contents

1 Introduction **4**

2 Physics: RLC vs. RLD **6**

3 Methods **12**

4 Results **19**

4.1 RLC 19

4.2 RLD 22

4.3 The Feigenbaum Constant 24

5 Discussion **25**

6 Additional Data Tables **26**

List of Figures

1 Example of attractors in phase spaces for different values of frequency analyzed RLD Circuit. (Gebara, 2021) 4

2 Schematic of the RLC Circuit with a real inductor representation 6

3 Schematic of our RLD Circuit 8

4 Schematic of the RLD Circuit with a real diode representation 10

5 Qualitative Schematic of the RLC/RLD Circuit 12

6 Physical image of RLC setup 13

7 Waveform of RLC at resonance 14

8 FFT of RLC resonance peak 14

9 Progression image of output signal (blue) and input signal (yellow). From left to right we see the our output signal translate and grow as it approaches our resonant frequency. 15

10 RLD Progression Linear Region Image 1: Left side of resonance peak; about 50kHz away from resonance. 17

11 RLD Progression Linear Region Image 2: Resonance peak 17

12 RLD Progression Linear Region Image 3: Right side of resonance peak; about 30kHz away from resonance. 17

13 Waveform at low frequency high input voltage. Output is a half wave signal presumably clipped by the diode. 18

14 FFT and Waveform progression images of the Road to Chaos. (Left) Contains harmonics of the driving frequency. (Middle) Shows sub-harmonics of the driving frequency. (Right) Chaos in the form of spectrum-like frequencies and non-periodic waveforms. 18
15 FFT and Waveform snapshot of RLD. Revealing chaos in the form of non-periodic signals and and spectrum-like frequency response. Live motion is volatile while input voltage and driving frequency is fixed. 19
16 RLC Graph of Output Voltage Vs. ω. Fitted values for ω_0 and Γ. 20
17 RLC Graph of Output Voltage Vs. ω. Fitted values for R,L and C. 20
18 RLC Graph of Phase angle Vs. ω. Fitted Values ω_0, Γ, L,C, and R. Blue and magenta fits are shown overlapping. 21
19 RLD Graph of Output Voltage Vs. ω. Fitted values for ω_0 and Γ. 22
20 RLD Graph of Output Voltage Vs. ω. Fitted values for R,L and C. 22
21 RLD Graph of Phase angle Vs. ω. Fitted Values ω_0, Γ, L,C, and R. Blue and magenta fits are shown overlapping. 23

List of Tables

1 Table of all components used and their Uncertainties. 13
2 Table of 13 raw RLC values and uncertainties taken from the oscilloscope. 15
3 Table of 13 propagated RLC values. Using those from Table.2 and their propagation equations. 16
4 Table of fit values for Figure 16 17. 20
5 Table of statistical values for Figure 16 17. 20
6 Table of fit values for Figure 18. 22
7 Table of statistical values for Figure 18. 22
8 Table of fit values for Figure 19, 20, and 21. 23
9 Table of statistical values for Figure 19, 20, and 21. 23
10 Table of additional Error Sources 25
11 Table of 13 raw RLD values and uncertainties taken from the oscilloscope. 26
12 Table of 13 propagated RLD values. Using those from Table.11 and their propagation equations. 27

1 Introduction

What is chaos? Randomness? Disorder? On the surface, these conclusions seem reasonable. Many systems we observe in day-to-day life appear in this unpredictable and highly volatile way. We see it in the weather, in watching a child on a playground, or as Jeff Goldblum explains in Jurassic Park, in attempting to predict the route of a water droplet that fell on our wrist and proceeded down our arm. It is not evident that these physical phenomena could be modeled and shown to retain any underlying order or allow for predictability.

In fact, before 1960, instances where nonlinear models and their odd characteristics occurred, were often overlooked (Oestreicher, 2007). Henri Poincaré first noted the extreme sensitivity to initial conditions in his work with the n-body problem and revealed that dynamical systems (nonlinear) had unpredictable behaviors. However, neither he nor his predecessors pursued the subject. At the time, the topic was considered a waste. It wasn't until a century later that Edward Lorenz accidentally discovered the same initial condition sensitivity, which he later coined "The Butterfly Effect."

The butterfly effect is what we hear most often in the media, the idea that a butterfly's wing flap could cause a catastrophic event halfway around the world. The phrase was popularized, but soon after, mathematical physicists David Ruelle and Mitchell Jay Feigenbaum succeeded in changing the speculated predictions into theory (Propp, 2014). Ruelle contributed a statistical approach to chaos by introducing "strange attractors," a purely mathematical concept. As seen in **Figure.1**, the strange attractor reveals the pattern or tendencies our chaotic system will gravitate towards. Think of many droplets flowing into a pan with a narrow spout in the center. We may not be able to predict the trajectory of one individual droplet, but we aren't in the dark about the system dominating traits; the drops will inevitably pass into the spout. Similarly, this reasoning is used in applications, as mentioned in our first paragraph. Proving to the world chaos could be understood and result in practical application.

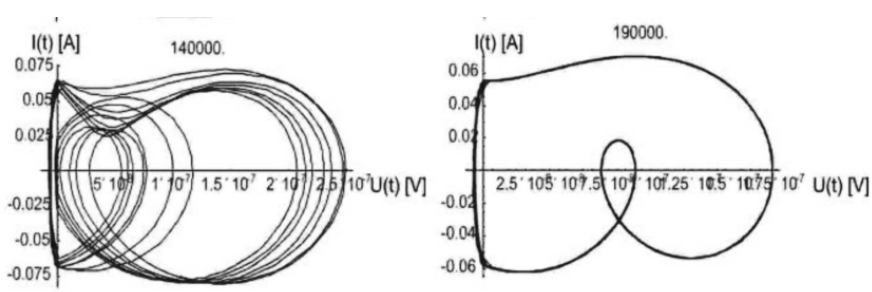

Figure 1: Example of attractors in phase spaces for different values of frequency analyzed RLD Circuit. (Gebara, 2021)

The most notable was Dr. Feigenbaum, who discovered the universal constant,

$$\delta = 4.669201609\ldots$$

which characterized the rate of period-doubling leading to chaos, aka the road to chaos; each doubling would occur exactly 4.699 times as quickly as the previous (Oestreicher, 2007). This period-doubling, better described as period-doubling bifurcation, is when slight changes to a system's parameters result in a new period double the original (Hanias, 2007). This bifurcation process continues into the chaos region, where initial conditions and outputs are no longer categorizable (Propp, 2014). We've seen that chaos, at least its route, is no longer random; it contains structures, predictable constants, and replicable results. Hence its revised name is deterministic chaos.

It is worth noting this particular constant is specific to functions that take the road to chaos by period-doubling bifurcation. Phenomenons that display this would be periodic and contain a bifurcation parameter. In our experiment, we will examine a nonlinear RLD circuit, which is known to exhibit period-doubling and have a bifurcation parameter. The following sections will describe the differential equations that govern this system and qualitatively speak about the different nonlinear regions. We will do this in conjunction with our analysis of an RLC circuit that serves as a comparable baseline for our RLD circuit at small oscillations. We will assume that our chaotic system should be well behaved at small enough oscillations, which are our initial conditions, and follow a predictable outcome.

2 Physics: RLC vs. RLD

This section describes our RLC and RLD components, their governing models, and how they come together as a differential equation. First consider **Figure 2**, which is a schematic of our base case RLC circuit. Note, in the figure, the dashed box about L and R_L represents our *real* inductor's model of internal resistance.

The known voltage models for R, L, and C are,

$$V_{R_T} = i(t) \cdot R_T$$
$$V_L = L \cdot \frac{di(t)}{dt}$$
$$V_C = \frac{Q}{C} = \frac{1}{C} \int i(t)\, dt$$

where R_T is the Thevenin resistance, L the inductance, C the capacitance, i(t) is the current as a function of time, and Q is the charge accumulated on the capacitor plates.

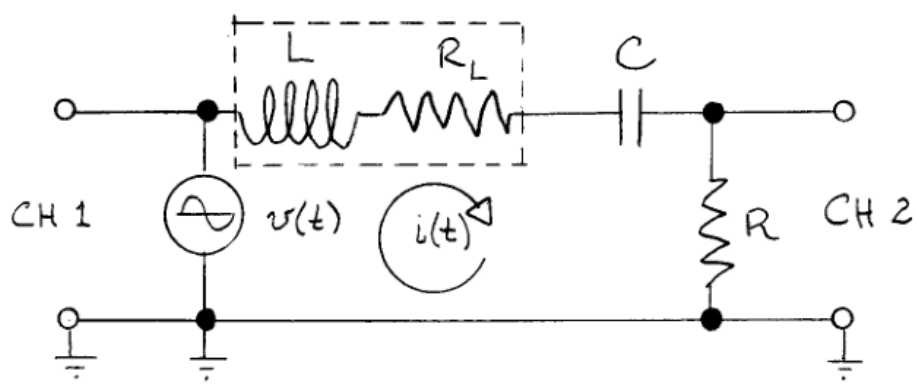

Figure 2: Schematic of the RLC Circuit with a real inductor representation

Next, we merge our models using Kirchhoff's Voltage Law, which states the sum of the voltage drops around any closed loop in a circuit must be zero. Our driving voltage is sinusoidal and supplied by our function generator (left-hand side connected to CH1) labeled as $v(t)$. The supply will cause a rise in voltage, whereas each other component will be a fall. We indicate this with positive and negative signs, respectively. To further specify our driver we will assign it an amplitude, V_0, and sine function, $v(t) = V_0 \cdot sin(\omega \cdot t - \phi)$. Where ω is our frequency and ϕ is the phase angle.

Kirchhoff's Voltage Law:

$$
\begin{aligned}
0 &= v(t) - V_{R_T} - V_L - V_C \\
v(t) &= V_R + V_L + V_C \\
V_0 \cdot \sin(\omega t - \phi) &= i(t)R + L\frac{di(t)}{dt} + \frac{1}{C}\int i(t)\, dt
\end{aligned}
$$

Let's address our resistance values. We do not include the resistance of the capacitor as we did for the inductor. Our manual omitted this, but we assumed it was due to the capacitor's short-like behavior at high frequencies. We found our theoretical resonant value to be above 10kHz and presumed this would be high enough to omit the possible resistance experienced by the capacitor. Yet, the 3db point of this arrangement resulted in $f_{3db} = \frac{1}{2\pi RC} = 159\text{kHz}$, which is much higher than 10kHz. Typically this means the arrangement would attenuate frequencies below 159kHz (see **Table.1** for values). We never reconciled this, but it's worth mentioning. To finalize we take the circuits Thevenin resistance $R_T = R + R_L$. Where R is our sensing resistor, which we measure across, and R_L is the inductor's modeled resistance.

$$
V_0 \cdot \sin(\omega t - \phi) = i(t)R_T + L\frac{di(t)}{dt} + \frac{1}{C}\int i(t)\, dt
$$

Let us simplify this by applying a time derivative, dividing by L, and defining some new terms. Let $\Gamma = \frac{R_T}{L}$ and $\omega_0 = \frac{1}{\sqrt{LC}}$ where ω_0 is our circuits resonant frequency.

$$
\frac{V_0\omega}{L}\cos(\omega t - \phi) = \frac{d^2 i(t)}{dt^2} + \Gamma\frac{di(t)}{dt} + \omega_0^2 i(t)
$$

In this differential form, we can conclude that our circuit is linear in i(t) and will result in solutions that obey the superposition principle (UCSC, 2022). The non-transient solutions, or solutions that depict the governing behavior, are as follows.

$$
i(t) = \frac{V_0\omega}{L\sqrt{(\omega_0^2 - \omega^2)^2 + \omega^2\Gamma^2}} \cdot \sin(\omega t - \phi) \tag{1}
$$

$$
v_R(t) = R \cdot i(t) = R \cdot \frac{V_0\omega}{L\sqrt{(\omega_0^2 - \omega^2)^2 + \omega^2\Gamma^2}} \cdot \sin(\omega t - \phi) \tag{2}
$$

$$
\tan(\phi) = \frac{\omega^2 - \omega_0^2}{\omega L} \tag{3}
$$

These equations can predict our resonant value, current, and voltage output. Consider the simplification at resonance i.e. $\omega = \omega_0$.

$$\phi = 0 \tag{4}$$

$$v_R(t) = R \cdot i(t) = R \cdot \frac{V_0}{R_T} \sin(\omega t) \tag{5}$$

Recall that our driving voltage is $v(t) = V_0 \sin(\omega t - \phi)$ indicating at this frequency, our input and output signals will be in phase, but the output will attenuate by a factor of $\frac{R}{R_T}$.

We will drive the circuit about its theoretical resonance and take several measurements of V_0, v_R, ω, and ϕ. Taking these values and their component's measured values, we can create a fit to see how well our measurements match our predictions. We want to show how our system, which linear models govern, has predictable and obtainable outcomes.

In contrast, consider the RLD circuit from **Figure.3**, where we replace the capacitor with a diode. The diode's current, ruled by Ebers-Moll's equation, is nonlinear in that its relationship with voltage is exponential.

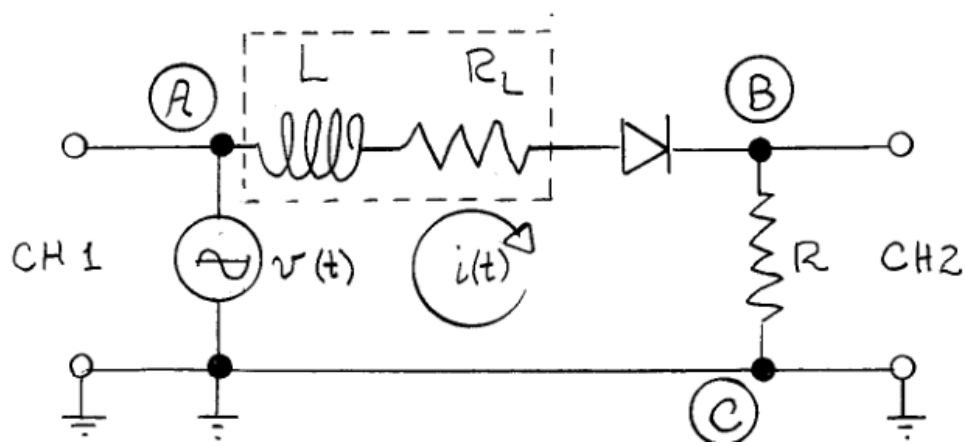

Figure 3: Schematic of our RLD Circuit

Ebers-Moll's Equation:

$$i(t) = i_R[exp(ev/kT) - 1] \tag{6}$$

Where $i(t)$ is the current in the loop, i_R is the reverse current (which depends on the parameters of the specific device), v is our output voltage, e is the charge on an electron $1.602 \cdot 10^{-19}$C, k is the Boltzmann's constant $1.38 \cdot 10^{-23} m^2 kgs^{-2} K^{-1}$, and T is the Temperature. At a room temperature of 294K the value $kT/e = 0.025$ volts (UCSC, 2022).

To examine all regions of our circuit, we may consider first what happens at small voltages by applying a Taylor expansion.

Expansion of e^x:

$$e^x = 1 + x + \frac{x^2}{2} + \dots$$

Where $x = \frac{e}{kT} \cdot v$. Clearly if our argument is squared so will v, meaning we may consider higher order terms as negligible.

$$i(t) = i_R \cdot \frac{e}{kT} \cdot v$$
$$i(t) = i_R \cdot \frac{1}{0.025} \cdot v$$

Rearranging this, we find our familiar Ohms law, implying at low voltages, our diode will behave as a linear resistor with resistance $R_d = \frac{0.025}{i_R}$. Insinuating that this is our linear region.

$$v = i(t) \cdot R_d = i(t) \cdot \frac{0.025}{i_R} \tag{7}$$

We still need to consider the internal capacitance of our diode. Since diodes are p-n junctions of semiconductor material, they contain depletion layers. Essentially, on either end of the diode, we will find material with an excess of either holes (positive-type) or electrons (negative-type) while also having a small gap/layer in the center. An electric field generates due to the p-type and n-type material sitting on either end of the depletion layer. Hence, acting as a capacitor. Therefore, at small enough voltages, we expect our circuit to exhibit similar behaviors to that of our RLC (UCSC, 2022). Also, we assume R_d can be neglected at high frequencies/ low voltages as current shorts through the capacitor, which behaves relatively constant.

As noted in the UCSC Physics 134 Manual, the diode's capacitance is always present.(46) Therefore, we include this in our updated schematic shown in **Figure.4**.

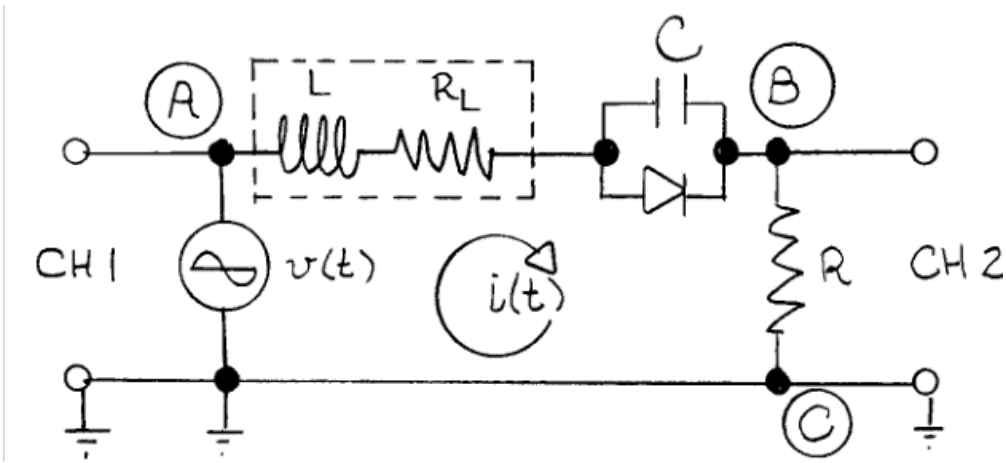

Figure 4: Schematic of the RLD Circuit with a real diode representation

What physically contributes to the chaos? It is assumed to be a consequence of un-recombined electrons and holes that crossed in the forward bias of the diodes p-n junction (Hanias, 2007). As we increase the voltage, leaving the linear region, we will impart higher charge buildup on in diode. However, our sinusoidal driver causes a struggle in the diode. Since the diode allows current in one direction, the quick alternating nature of the driver will inadvertently cause the state change to be incomplete. Meaning rather than returning to an initial state, say the moment the circuit was closed, it will need to begin at the state it managed to reach previously (Smith-King, 2014). The changing of initial parameters will continue until the circuit's voltage is lowered or turned off. Otherwise, chaos will ensue, and we will lose predictability. But, we are interested in this behavior, so we allow the system to evolve.

Finally, we construct the presumed nonlinear differential equation. Kirchhoff's voltage law accounts for the voltage of the loop as done previously. At the same time, Kirchhoff's current law will account for the parallel arrangement of the capacitor and diode. The current law states the algebraic sum of all currents entering and exiting a node must equal zero. So the current in the main loop should equal the sum of the currents flowing through the capacitor and diode.

The current through the capacitor and diode are $i_C = \frac{d}{dt}(V \cdot C)$ and $i_d = i_R[exp(ev/kT) - 1]$. Where i is the current of the main loop.

Kirchhoff's Current Law:

$$\begin{aligned} 0 &= i - i_C - i_d \\ i &= i_C + i_d \\ i &= i(v) \end{aligned}$$

We see $i(v)$, the implicit representation of our current, can be inverted for v, the drop across the diode. Giving us $v(i)$, which is the voltage drop across the parallel combination V_d. Also, our Thevenin resistance is as before $R_T = R + R_L$.

Kirchhoff's Voltage Law:

$$\begin{aligned} V_0 \sin(\omega t - \phi) &= V_L + V_{R_T} + V_d \\ V_0 \sin(\omega t - \phi) &= L\frac{di}{dt} + i \cdot R_T + v(i) \end{aligned}$$

Like before, we apply a derivative and divide by L.

$$\begin{aligned} \frac{V_0 \omega}{L} \cos(\omega t - \phi) &= \frac{d^2}{dt^2} i(v) + \frac{R_T}{L} \frac{d}{dt} i(v) + \frac{d}{dt} v(i) \\ \frac{V_0 \omega}{L} \cos(\omega t - \phi) &= \frac{d^2}{dt^2} i(v) + \frac{R_T}{L} \frac{d}{dt} i(v) + v'(i) \frac{d}{dt} i(v) \end{aligned}$$

At this moment, we can already see our familiar second-order differential equation. Except for the final term now contains nonlinear values—the expected characteristic that contrasts with our RLC circuit. No solution is provided but one can be derived for small input voltages.

3 Methods

In the following, we describe our procedure for collecting and analyzing data points. The wiring of our circuits is straightforward in that we followed the schematics from the previous section. An illustration and real image is presented in **Figure.5** and **Figure.6** respectively. Note, in **Figure.5** blue boxes describe the purpose of each wire or set of wires. Those connected to CH1 and CH2 measure our input voltage from the function generator and the output voltage across the resistor. Note that the input voltage is read after passing through the potentiometer, which attenuates the signal. In our second experiment, we require small inputs hence its need.

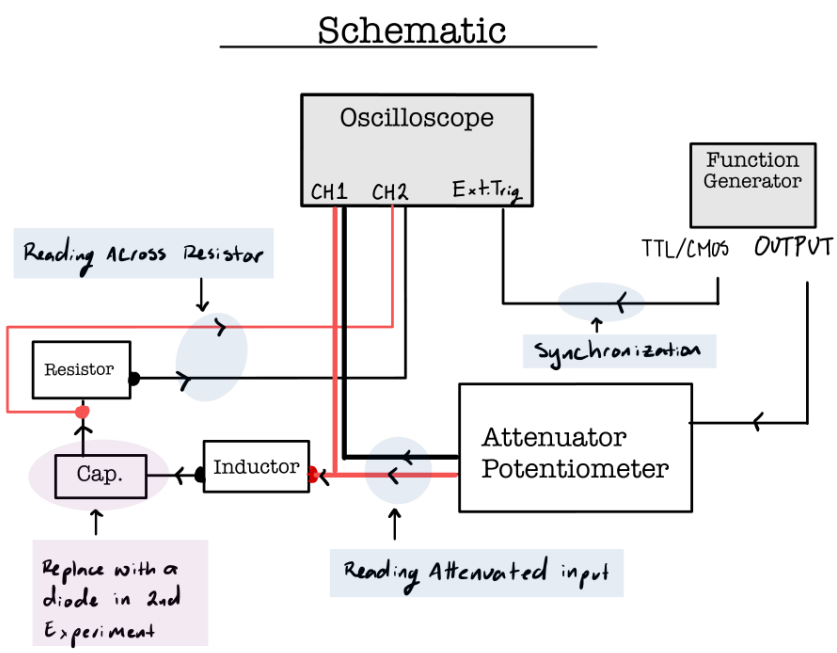

Figure 5: Qualitative Schematic of the RLC/RLD Circuit

Furthermore, the wire labeled as synchronization in **Figure.5** is precisely named. Connecting the oscilloscope's external trigger with the function generator's TTL/CMOS channel gives a synchronized trigger reading needed for a steady image during our sweep of the nonlinear regions (Tektronixs, 2003). For a complete description of our parts, see **Table.1** which contains a full list of materials, their descriptions, uncertainties, and references.

Figure 6: Physical image of RLC setup

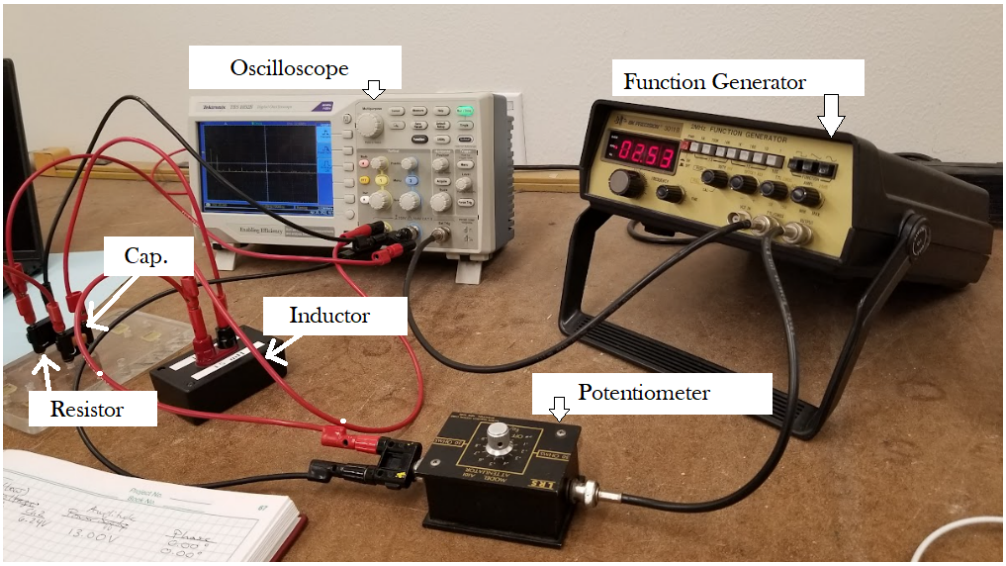

Table 1: Table of all components used and their Uncertainties.

Item	Description	Uncertainty Associated	Add.Info
Fluke 77	Multimeter	(320.0,3200)Ohm: (+/- 0.5% + 2, +/- 0.5% + 1)	(FLUKE, 1991)
BK Precision 810C	Capacitance Meter	Csig = +/-(0.5%rdg + 1dgt)	(BK Precision, 2001)
Tektronix TBS 1052B	Digital Oscilloscope	Vertical, Horizontal: +/- 3%, 50 ppm	(Tektronix, 2003)
1N4004 Diode	Reverse current at room temp	$i_R = (0.05 + / - .02)uA$	(VISHAY, 2020)
1N4004 Diode	Resistance	$R_d = 0.025/i_R = 50kOhms$	(VISHAY, 2020)
BK Precision 3011B	2MHz Function Generator	Transferred to Oscilloscope reading	(BK Precision,2002)
Potentiometer	Attenuates the output signal	n/a	n/a
Resistor 1 (RCL)	R1 = 98.8 Ohms	R1Sig = +/- 2.494 Ohms	M.Meter
Capacitor (RCL)	C1 = 10.08 nF	C1Sig = +/- 1.05 nF	C.Meter
Inductor 1 (RCL)	L1 = 15 mH	L1Sig = +/- 1.0 mH	n/a
Inductor Resistance 1	RL1 = 103.4 Ohms	RL1Sig = +/- 2.517 Ohms	M.Meter
Resistor 2 (Nonlinear)	R2 = 3,300 Ohms	R2Sig = +/- 17.5 Ohms	M.Meter
Inductor 2 (Nonlinear)	L2 = 25 mH	L2Sig = +/- 5.0 mH	n/a
Inductor Resistance 2	RL2 = 151 Ohms	RL2Sig = +/- 2.755 Ohms	M.Meter

The measurements listed in **Table.1** were taken with our Fluke 77 Multimeter and BK Precision Capacitance meter. Their documented uncertainties are also listed in **Table.1**.

To show the predictability of our models, we measure the expected resonance frequencies of both circuits. In **Figure.7**, we see our predicted waveform characteristics. The input and output signals are in phase, and from our peak-peak readings, we can measure the expected attenuation from **Equation.5**.

Example Calculation of **Equation.5** based on the values in **Figure.7** and **Table.1**:

$$
\begin{aligned}
|v_R| &= |R \cdot \frac{V_0}{R_T} \sin(\omega t)| \\
|v_R| &= R \cdot \frac{V_0}{R_T} \\
|v_R| &= R1 \cdot \frac{V_0}{R1 + RL1} \\
|\frac{(pk-pk)_{blue}}{2}| &= 98.8 \cdot \frac{(pk-pk)_{yellow}}{2} \cdot \frac{1}{98.8 + 103.4} \\
|\frac{6.16}{2}| &= 98.8 \cdot \frac{146}{2} \cdot \frac{1}{998.8 + 103.4} \\
|v_R| &= 3.08 \neq 35.7
\end{aligned}
$$

Our calculated value of $v(t)$ is off by 10. We speculate this is due to the attenuation setting on the oscilloscope. It was set to x10 attenuation and overlooked until after the experiment concluded. With this in mind, we acknowledged the above value is near the result we expected. Calculations such as the one above affirm our resonance peak but are not used as a fit model.

Figure 7: Waveform of RLC at resonance

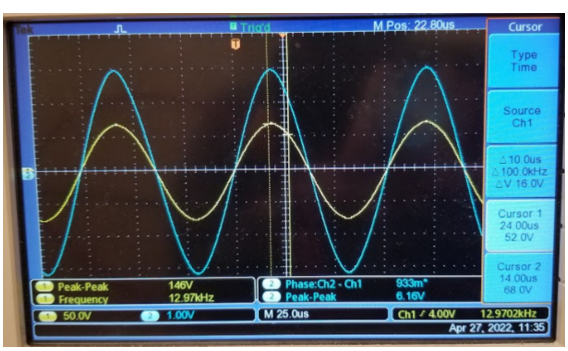

Figure 8: FFT of RLC resonance peak

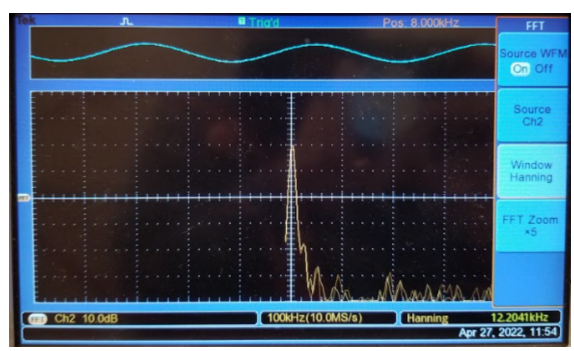

In **Figure.9**, we see a progression image showing how the output signal translates with increasing frequency. From left to right in our image, the output attenuates as it moves away from the resonant frequency and increases to a maximum at the resonance (center image). **Table.2** contains 13 measurements from our sweep of input voltage (VIn), output voltage (VOut), frequency (f), the time difference between waves (Td), period of out output wave (T), and their respective uncer-

tainties. We set the oscilloscope to average 128 waveforms and then took measurements from the display screen as seen in **Figure.7**. Then we select the FFT setting, which performs a fast Fourier transform on our waveform and converts it to a frequency domain (Tektronix, 2003). Allowing us to view the frequency of our waveform. **Figure.8** displays the resonant peak and waveform. We can adjust the frequency in the FFT display to see the peak better while watching it as it reaches its greatest amplitude.

Figure 9: Progression image of output signal (blue) and input signal (yellow). From left to right we see the our output signal translate and grow as it approaches our resonant frequency.

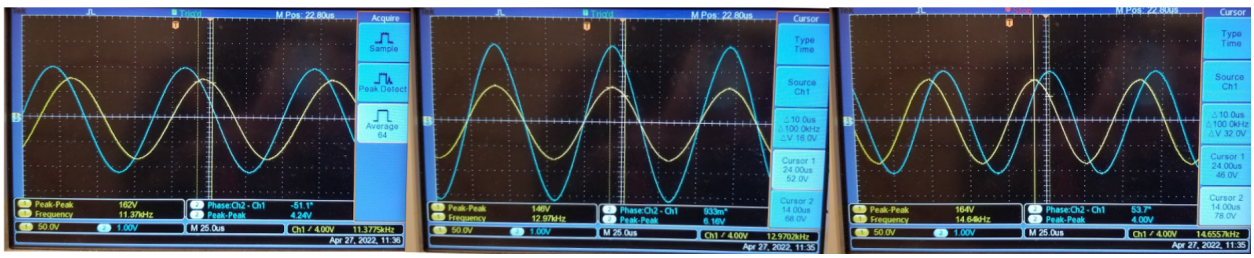

Table 2: Table of 13 raw RLC values and uncertainties taken from the oscilloscope.

VIn (V)	σ_{Vin} (V)	VOut (V)	σ_{Vout} (V)	f (Hz)	σ_f (Hz)	T (s)	σ_T (s)	Td (s)	σ_{Td} (s)
83	1	1.62	0.04	10650.00	120	9.40E-05	1.00E-06	1.70E-05	1.00E-06
82	1	2.00	0.04	11220.00	120	8.90E-05	1.00E-06	1.40E-05	1.00E-06
79	1	2.44	0.04	11490.00	120	8.50E-05	1.00E-06	8.00E-06	1.00E-06
77	1	2.68	0.04	12100.00	120	8.30E-05	1.00E-06	7.00E-06	1.00E-06
75	1	2.84	0.04	12360.00	120	8.10E-05	1.00E-06	6.00E-06	1.00E-06
74	1	3.04	0.04	12830.00	120	7.70E-05	1.00E-06	3.00E-06	1.00E-06
73	1	3.08	0.04	12930.00	120	7.70E-05	1.00E-06	3.00E-08	1.00E-06
73	1	3.04	0.04	13080.00	120	7.60E-05	1.00E-06	1.00E-06	1.00E-06
74	1	3.00	0.04	13280.00	120	7.50E-05	1.00E-06	3.00E-06	1.00E-06
77	1	2.64	0.04	13770.00	120	7.20E-05	1.00E-06	6.00E-06	1.00E-06
80	1	2.36	0.04	14100.00	120	7.10E-05	1.00E-06	8.00E-06	1.00E-06
80	1	2.20	0.04	14340.00	120	7.00E-05	1.00E-06	9.00E-06	1.00E-06
82	1	2.00	0.04	14660.00	120	6.90E-05	1.00E-06	1.00E-05	1.00E-06

From **Table.2** we calculate phase and angular frequency along with their error propagation. Their formulas are as follows and values are found in **Table.3**.

Phase angle ϕ and its uncertainty calculation σ_ϕ:

$$\phi = 360 \cdot \frac{Td}{T}$$
$$\sigma_\phi^2 = \left(\frac{\partial \phi}{\partial Td}\right)^2 \cdot \sigma_{Td}^2 + \left(\frac{\partial \phi}{\partial T}\right)^2 \cdot \sigma_T^2$$
$$\sigma_\phi^2 = \left(360 \cdot \frac{1}{T}\right)^2 \cdot \sigma_{Td}^2 + \left(360 \frac{Td}{T^2}\right)^2 \cdot \sigma_T^2$$

Angular frequency ω and its uncertainty calculation σ_ω:

$$\omega = 2 \cdot \pi \cdot f$$
$$\sigma_\omega^2 = (2\pi)^2 \cdot \sigma_f^2$$

Table 3: Table of 13 propagated RLC values. Using those from Table.2 and their propagation equations.

ω (Hz)	σ_ω (Hz)	ϕ (deg)	σ_ϕ (deg)
66915.92	753.98	-65	3.89
70497.34	753.98	-57	4.09
72193.8	753.98	-34	4.25
76026.54	753.98	-30	4.35
77660.17	753.98	-27	4.45
80613.27	753.98	-14	4.67
81241.59	753.98	0	4.67
82184.06	753.98	5	4.73
83440.7	753.98	14	4.80
86519.46	753.98	30	5.01
88592.91	753.98	41	5.10
90100.88	753.98	46	5.18
92111.5	753.98	52	5.27

An identical process is taken for the RLD circuit's linear region. The values are found in **Table.11** and **Table.12** located in the *Addition Data Table* section of this report. The following pages have enlarged images of our circuit's different regions. The first three images are of the linear region. However, we already see some non-linearity at lower frequencies in the first image.

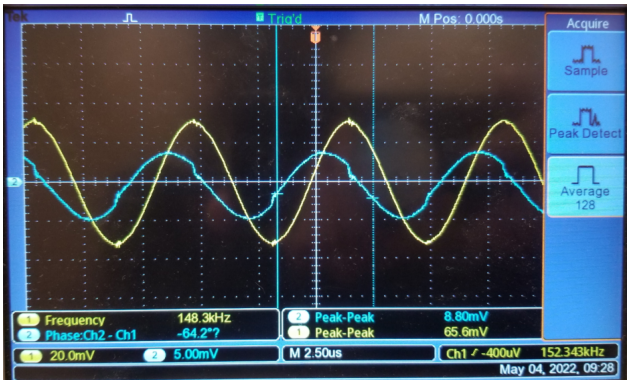

Figure 10: RLD Progression Linear Region Image 1: Left side of resonance peak; about 50kHz away from resonance.

Figure 11: RLD Progression Linear Region Image 2: Resonance peak

Figure 12: RLD Progression Linear Region Image 3: Right side of resonance peak; about 30kHz away from resonance.

We included the following image to show the nonlinear region, which we can find at high input voltages or by lowering the driving frequency. **Figure.13** specifically resembles a half-wave signal. We theorize this is due to the diode's ability to return to an equilibrium state and block the reverse bias current resulting in a clipped waveform.

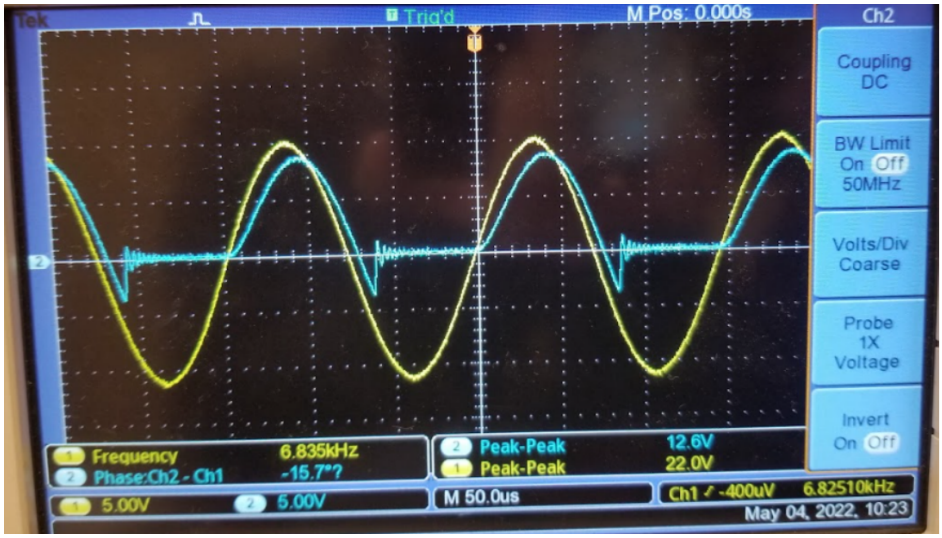

Figure 13: Waveform at low frequency high input voltage. Output is a half wave signal presumably clipped by the diode.

Next, we have another progression image that depicts the road to chaos by period-doubling. **Figure.15** is an enlarged image of the chaos region. We discovered period-doubling was only visible when the signal became unsteady. Additionally, we do not have adequate images of period-doubling to display due to our misunderstanding of the material at the time.

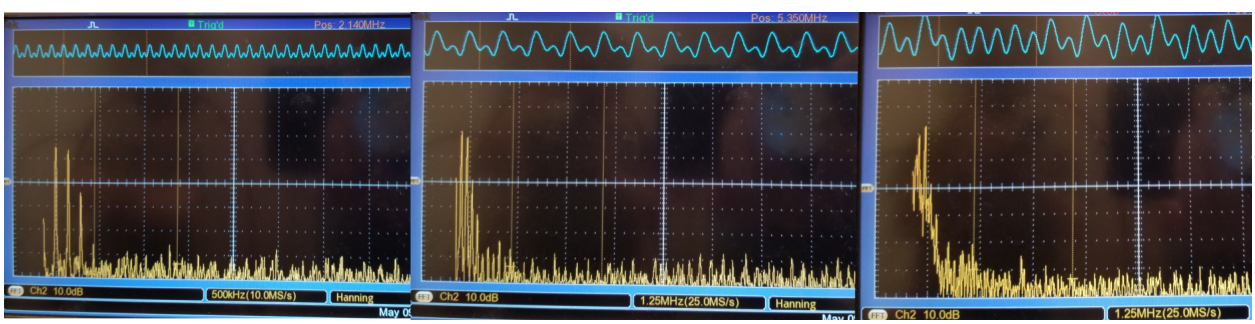

Figure 14: FFT and Waveform progression images of the Road to Chaos. (Left) Contains harmonics of the driving frequency. (Middle) Shows sub-harmonics of the driving frequency. (Right) Chaos in the form of spectrum-like frequencies and non-periodic waveforms.

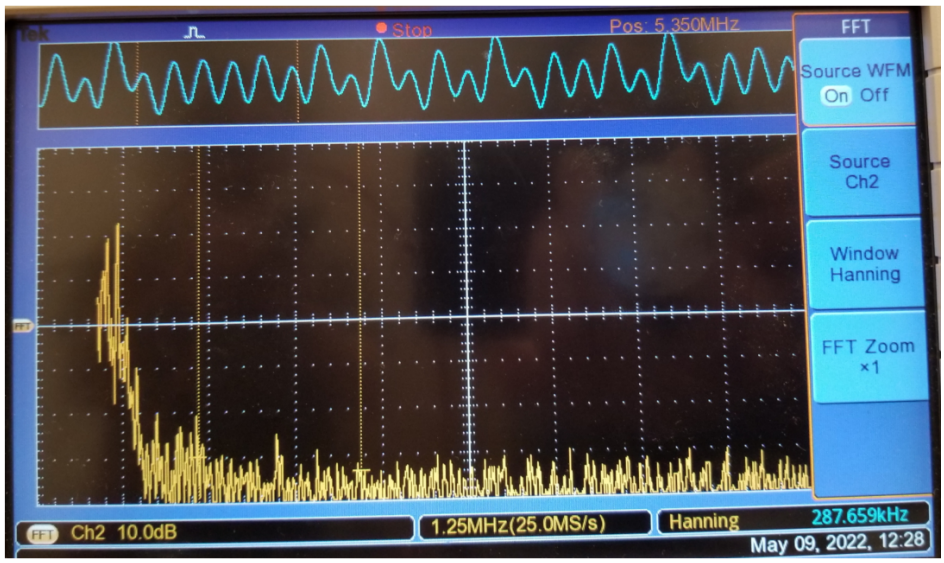

Figure 15: FFT and Waveform snapshot of RLD. Revealing chaos in the form of non-periodic signals and and spectrum-like frequency response. Live motion is volatile while input voltage and driving frequency is fixed.

4 Results

The following contains tables of key values showing our predicted linear regions, along with fitted graphs, Chi^2, and p-values. Concluding with images of a route to Chaos and a small calculation of the Feigenbaum constant derived from our period-doubling bifurcation parameter (VIn).

4.1 RLC

All plots are fit with scipy.optimize.curve_ fit() with parameters absolute_ sigma = True and sigma = σ_{V_out} from **Table.2**. **Figure.16** is fit **Equation.8** where V_0 was fixed to 7.6 volts.

$$v_R(t)_{Max} = R \cdot \left(\frac{V_0 \omega}{L\sqrt{(\omega_0^2 - \omega^2)^2 + \omega^2 \Gamma^2}} \right) \tag{8}$$

Figure.17 is fit **Equation.9** with fixed variables $V_0 = 7.6$ volts and $R_L = 103.4$ Ohms.

$$v_R(t)_{Max} = R \cdot \left(\frac{V_0 \omega}{L\sqrt{((\frac{1}{\sqrt{LC}})^2 - \omega^2)^2 + \omega^2 (\frac{R+R_L}{L})^2}} \right) \tag{9}$$

Figure 16: RLC Graph of Output Voltage Vs. ω. Fitted values for ω_0 and Γ.

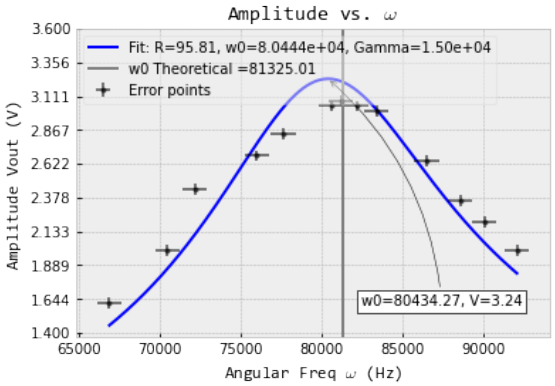

Figure 17: RLC Graph of Output Voltage Vs. ω. Fitted values for R,L and C.

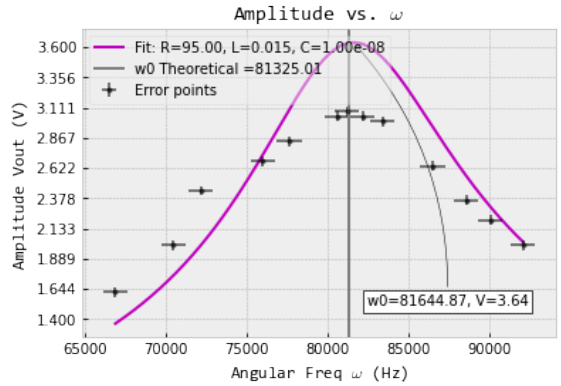

Table 4: Table of fit values for Figure 16 17.

Symbol	Fit	Uncertainty	Theoretical	Units
Figure 16				
R	95.8	1.32	99.8	Ohms
ω_0	80443	91.7	81325	Hz
Γ	14999	263.6	13546	
Figure 17				
R	95	2.97	99.8	Ohms
L	0.015	2.75E-05	0.015	H
C	1.00E-08	2.05E-10	1.01E-08	F

Table 5: Table of statistical values for Figure 16 17.

Figure 16		Figure 17	
Name	Value	Name	Value
Chi^2	211.8	Chi^2	1105
Degrees of Freedom	10	Degrees of Freedom	10
Reduced Chi^2	21.1	Reduced Chi^2	110
CDF	1	CDF	1
p-value	0	p-value	0

Two fits were used due to continued issues in the uncertainty. Our values for Chi^2 reveal this difficulty in that we have a p-value of zero, see **Table.5**. Indicating we found evidence to reject our null hypothesis. However this is unlikely and we conclude the measurements were done poorly. The result is now taken qualitatively from the images shown in *Methods*. Our resonance peak did occur near the theoretical value.

Theoretical ω_0 and f_0:

$$\begin{aligned}\omega_0 &= \frac{1}{\sqrt{LC}} \\ &= 81325Hz \\ f_0 &= \frac{\omega_0}{2\pi} \\ &= 12943Hz\end{aligned}$$

In *Methods*, **Figure.7** contains a value close to 12kHz.

Figure 18: RLC Graph of Phase angle Vs. ω. Fitted Values ω_0, Γ, L,C, and R. Blue and magenta fits are shown overlapping.

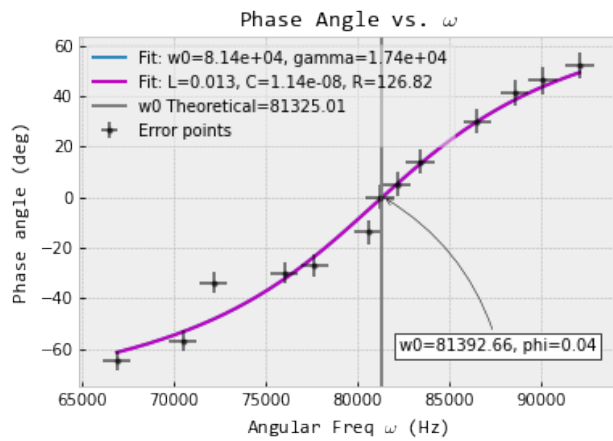

The two modeled functions are,

$$\phi = \tan^{-1}\left(\frac{\omega^2 - \omega_0^2}{\omega \cdot \Gamma}\right) \tag{10}$$

$$\phi = \tan^{-1}\left(\frac{\omega^2 - \frac{1}{LC}}{\omega \cdot \frac{R_T}{L}}\right) \tag{11}$$

where **Equation.11** has R_L fixed to 103.4 Ohms.

We had more success with our phase angle function but only in comparison to our magnitude function. **Table.6** and **Table.7** outline our fit values.

Table 6: Table of fit values for Figure 18.

Symbol	Fit	Uncertainty	Theoretical	Units
ω_0	81386	272	81325	Hz
Γ	17426	999	13546	
R	126.8	8888863505	99.8	Ohms
L	0.0132	5.10E+03	0.015	H
C	1.14E-08	4.40E-03	1.01E-08	F

Table 7: Table of statistical values for Figure 18.

Name	Value
Chi^2	18
Degrees of Freedom	10
Reduced Chi^2	1.82
CDF	0.948
p-value	0.051

4.2 RLD

We had similar issues with our chaos circuit. The following plots are fit with the same equations as before.

Figure 19: RLD Graph of Output Voltage Vs. ω. Fitted values for ω_0 and Γ.

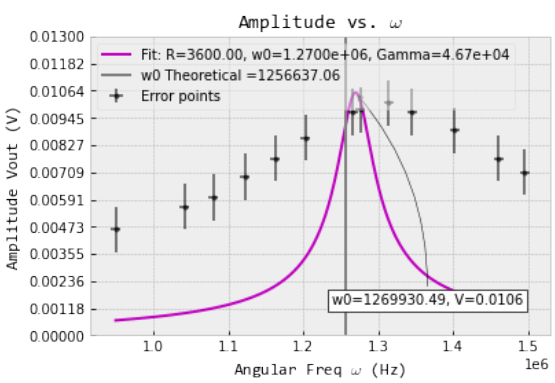

Figure 20: RLD Graph of Output Voltage Vs. ω. Fitted values for R,L and C.

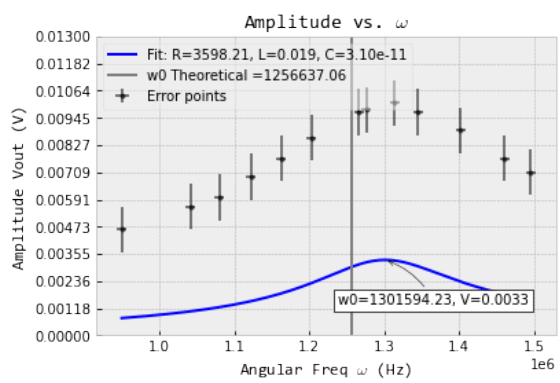

Figure 21: RLD Graph of Phase angle Vs. ω. Fitted Values ω_0, Γ, L,C, and R. Blue and magenta fits are shown overlapping.

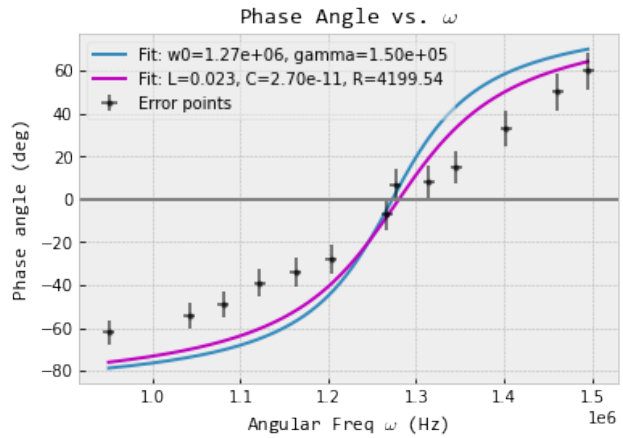

Table 8: Table of fit values for Figure 19, 20, and 21.

Symbol	Fit	Uncertainty	Theoretical	Units
Figure 19				
ω_0	81386	272	81325	Hz
Γ	17426	999	13546	
Figure 20				
R	126.8	8888863505	99.8	Ohms
L	0.0132	5.10E+03	0.015	H
C	1.14E-08	4.40E-03	1.01E-08	F
Figure 21				
ω_0	1272859	5169	81325	Hz
Γ	149999	14506	13546	
R	4199	1.47E-10	99.8	Ohms
L	0.0225	3.73E-04	0.015	H
C	2.70E-12	1.11E-12	1.01E-08	F

Table 9: Table of statistical values for Figure 19, 20, and 21.

Figure 19		Figure 20		Figure 21	
Name	Value	Name	Value	Name	Value
Chi^2	339	Chi^2	449	Chi^2	100
Degrees of Freedom	10	Degrees of Freedom	10	Degrees of Freedom	10
Reduced Chi^2	33.9	Reduced Chi^2	44.9	Reduced Chi^2	10.03
CDF	1	CDF	1	CDF	1
p-value	0	p-value	0	p-value	0

Again we must resort to the qualitative conclusions from **Figure.11** and our theoretical frequency.

$$f_0 = \frac{\omega_0}{2\pi} = 200kHz$$

4.3 The Feigenbaum Constant

As a final note we will include a brief method to measuring the Feigenbaum Constant, δ, with an example taken form our measurement. However Images are not shown.To measure δ we only need our bifurcation parameter VIn and the following formula.

$$\delta = \frac{a_{n-1} - a_{n-2}}{a_n - a_{n-1}}$$

Where a is our input voltage values measured at moments were bifurcation occurs. Our equation requires at minimum 3 successive bifurcations. We found the best method to identify these values is to use the FFT display. When a new bifurcation or set of harmonics/sub harmonics are visible we found it was best to find their max amplitude just prior to the next bifurcation. At that the highest amplitude we revert the display to the wave form and record the peak to peak value and divide by 2.

In one attempt we found the following inputs in increases order 2.24V,4.04V, and 4.48V. Our measured constant was,

$$\delta = \frac{4.04 - 2.24}{4.48 - 4.04} = 4.09$$

Which is a 12% error for one attempt. This calculation is not rigorous but is included in hopes to share the result for future labs involving the RLD chaos circut.

5 Discussion

Several issues impeded our ability to produce adequate data. Some are outlined in **Table.10**. We recognize now that measurements around the resonance frequency require very fine steps to produce a fine peak in addition to several points a distance away from the peak. Values taken a distance away should, in theory, give us a better fit, as they will fall into either the inductor or capacitor's dominating characteristic. Moreover, we did not include or have time to look into the behavior of this circuit at higher frequencies. Our experiment revealed that regardless of the input voltage at about 500 kHz, the signal was completely attenuated, and at higher frequencies, the output was steady and sinusoidal. We speculated this was due to the inductor but did not have time to investigate. Above all else, we did not properly label the images taken at the time of capture, providing unnecessary difficulty for analysis. This was also due to not properly understanding how to find the route to chaos until the last day of data capture. In the future, a more detailed account should be taken when collecting images, along with a wider spread of data points. However, we could incorporate the Feigenbaum constant, if only briefly, which was not accounted for in the lab manual.

Table 10: Table of additional Error Sources

Item	Description	Uncertainty Contributions
Diode Capacitance	Formula: C = $\frac{1}{L\omega^2}$	Assumed this was the equation to use, vs. V=IR = Q/C because we did not have a time region.
Attenuation	RCL reading with x10 Attenuation	Was set to X10 and was advised to have x1 but we did not redo the experiment at x1. Fixed for Non-linear
Inductors	Black box and coil	No documentation. B.box: label, coil: Value from manual
Oscilloscope	Reading any on screen value	Unsure how to utilize the rating, gave uncertainty based on visual cues.
Function Generator	Settings (TTL/Cmos to Ext. Trig)	Assumed previously set correctly i.e. the synchronization of the Oscilloscope to the F.Generator
Resonant Measurements	approx. 10 reading about Resonance	Fine dials were still too aggressive. Measurements were not as precise as we would like.

6 Additional Data Tables

Table 11: Table of 13 raw RLD values and uncertainties taken from the oscilloscope.

VIn (V)	σ_{Vin} (V)	VOut (V)	σ_{Vout} (V)	f (Hz)	σ_f (Hz)	T (s)	σ_T (s)	Td (s)	σ_{Td} (s)
0.03275	0.001	0.00460	0.001	151200.00	1000	6.40E-06	1.00E-07	1.10E-06	1.00E-07
0.03280	0.001	0.00560	0.001	165800.00	1000	6.00E-06	1.00E-07	9.00E-07	1.00E-07
0.03280	0.001	0.00600	0.001	171900.00	1000	5.90E-06	1.00E-07	8.00E-07	1.00E-07
0.03280	0.001	0.00690	0.001	178600.00	1000	5.60E-06	1.00E-07	6.00E-07	1.00E-07
0.03275	0.001	0.00770	0.001	185100.00	1000	5.30E-06	1.00E-07	5.00E-07	1.00E-07
0.03240	0.001	0.00860	0.001	191500.00	1000	5.20E-06	1.00E-07	4.00E-07	1.00E-07
0.00342	0.001	0.00970	0.001	201600.00	1000	5.00E-06	1.00E-07	1.00E-07	1.00E-07
0.03280	0.001	0.00980	0.001	203200.00	1000	5.00E-06	1.00E-07	1.00E-07	1.00E-07
0.03280	0.001	0.01010	0.001	209200.00	1000	4.80E-06	1.00E-07	1.00E-07	1.00E-07
0.03280	0.001	0.00970	0.001	214100.00	1000	4.70E-06	1.00E-07	2.00E-07	1.00E-07
0.03280	0.001	0.00890	0.001	223200.00	1000	4.40E-06	1.00E-07	4.00E-07	1.00E-07
0.03280	0.001	0.00770	0.001	232500.00	1000	4.30E-06	1.00E-07	6.00E-07	1.00E-07
0.03280	0.001	0.00710	0.001	238000.00	1000	4.20E-06	1.00E-07	7.00E-07	1.00E-07

Table 12: Table of 13 propagated RLD values. Using those from Table.11 and their propagation equations.

ω (Hz)	σ_ω (Hz)	ϕ (deg)	σ_ϕ (deg)
950017	6283.19	-62	5.707
1041752	6283.19	-54	6.067
1080079	6283.19	-49	6.157
1122176	6283.19	-39	6.465
1163017	6283.19	-34	6.822
1203229	6283.19	-28	6.943
1266690	6283.19	-7	7.201
1276743	6283.19	7	7.201
1314442	6283.19	8	7.501
1345229	6283.19	15	7.666
1402406	6283.19	33	8.215
1460840	6283.19	50	8.453
1495398	6283.19	60	8.689

References

[1] BK Precision 810C. (2001). *Operating Instructions Capacitance Meter*. Maxtec International Corp.

[2] BK Precision. (2002). *Instruction Manual, 2MHz Digital Display Function Generator*. Maxtec International Corp. (https://www.bkprecision.com/products/discontinued/3011B-2-mhz-func-gen-w-coarse-fine-discontinued.html)

[3] FLUKE. (1991). *Series II Multimeter, Service Manual*.John Fluke Mtg, Inc.

[4] Gebara. P., Gebara. M. (2021). Frequency-Dependent Chaotic Behavior in RLD Circuit. *ACTA Physica Polonica A, Vol.139* (No.5), 522-544.

[5] Hanias. M.P, Averinos. Z., Tombras. G.S. (2007) Period doubling, Feigenbaum constant and time series prediction in an experimental chaotic RLD circuit. *Science Direct Chaos, Solitons and Fractals 40*, 1050-1059.

[6] King-Smith. M. (2014). A Nonlinear Electrical Circuit Exhibiting Doubling Bifurcation and Chaotic Behavior. *Physics Department, The College of Wooster, Wooster, Ohio*.

[7] Oestreicher, C. (2007). A history of chaos theory. *Dialogues in Clinical Neuroscience*, 9(3), 279–289.

[8] Propp.S. (2014).Period Doubling Route to Chaos in a RLD Circuit. *Physics Department, The College of Wooster, Wooster, Ohio*.

[9] Tektronix. (2003) *TBS1000B and TBS1000B-EDU Series Digital Storage Oscilloscopes User Manual*. Tektronix, Inc. (www.tek.com)

[10] U.C Santa Cruz. (2022) *Advanced Physics Laboratory*

[11] VISHAY. (2020) *1N4001,..,1N4004... Vishay General Semiconductor*. Vishay Intertechnology, Inc. (www.vishay.com)